EUROPEAN ORGANIZATION FOR NUCLEAR RESEARCH

CERN/EP 82-18
18 February 1982

FIRST RESULTS FROM THE SPS COLLIDER

UA5 Collaboration
Bonn-Brussels-Cambridge-CERN-Stockholm

Presented by R.B. Meinke*

Physikalisches Institut, Bonn University, Germany

ABSTRACT

First results from experiment UA5 at the CERN SPS collider studying $p\bar{p}$ collisions at $\sqrt{s}$ = 540 GeV are presented[1]. The central region pseudorapidity density is 3.0 ± 0.1 for non-diffractive events. The FWHM of the observed pseudorapidity distribution is narrower than expected from a simple extrapolation of ISR data which can be interpreted as an increase in the mean p_t for hadron production. A value of 27.4 ± 2.0 is obtained for the mean charged multiplicity $\langle n_{ch} \rangle$ of produced hadrons. This is not in disagreement with an extrapolation using a quadratic fit in ℓns to previous lower energy data up to ISR energies, but excludes an $s^{1/4}$ or stronger dependence of $\langle n_{ch} \rangle$ on s. Correlations between charged particles of positive and negative c.m.s. pseudorapidity have been analysed. In contrast to ISR energies, where long range correlations have been found to be small, they appear to be as important as short range correlations at collider energies. Preliminary results on correlations between charged particles and photons over a limited acceptance ($\Delta|\eta| < 1$, $\Delta\phi = \pi/2$) in the central region of pseudo-rapidity are given.

APPARATUS

Streamer chamber system

A schematic layout of the UA5 detector[2] while installed in the LSS4 experimental area of the SPS collider is shown in fig. 1. Two 6 m long streamer chambers were placed one above and one below an elliptical beam pipe of 0.4 mm stainless steel, such that the visible volumes of the chambers were $\lesssim$ 9 cm apart. Lead-glass converter plates with a thickness of 1 radiation length are built into the sensitive volumes at the ends and the sides of one of the chambers as shown in fig. 1. Each chamber was viewed by three stereoscopic cameras: a main camera at each end viewing slightly more than half of the chamber at a demagnification of 50, and a central supplementary camera viewing the whole chamber at a demagnification of 80. Image

Presented at the 2nd Topical Conference on Forward Collider Physics
December 1981, Madison, Wisconsin, USA

(*) Presently at CERN.

intensifier tubes of gain ∿ 2000 were used with all cameras allowing us to photograph small streamers of 5-10 mm length. The resulting homogeneity of the chambers gave good track quality over the whole length and charged particles could be studied with pseudorapidities ($\eta = -\ell n \tan\theta/2$) $|\eta| \lesssim 5$ limited by the geometrical acceptance as shown in fig. 2. The spatial resolution was found to be 1-2 mm and the excellent two-track resolution of about 2 mm allowed one even to identify and study narrow pairs from photon conversions. The detector has no magnetic field, so the tracks in our streamer chambers are straight lines spreading out radially from the interaction point.

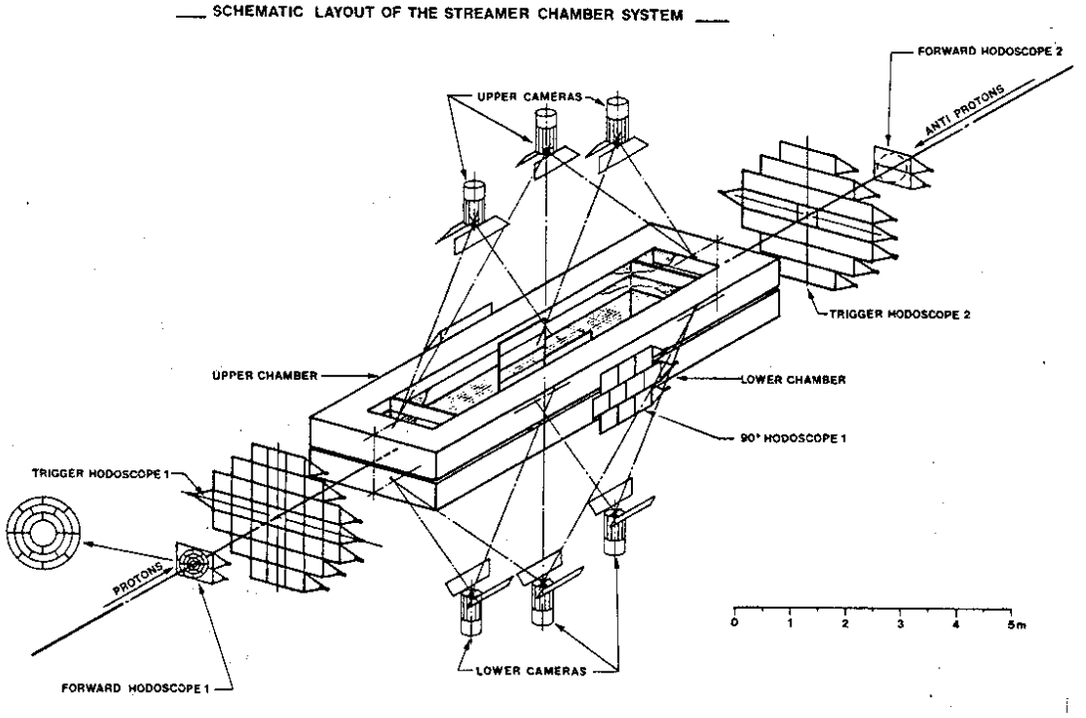

Fig. 1

Trigger

To trigger on as large a fraction as possible of the inelastic $p\bar{p}$ cross section six planes of scintillation counter hodoscopes have been used. They are located at the ends and the sides of the streamer chambers as indicated in fig. 1. The two counter planes at each end form "arm 1" and "arm 2" of the trigger system with the two planes in each arm being away 4.5 m and 5.5 m respectively from the centre of the apparatus.

An event trigger demanded at least one hit in each arm in coincidence ($n_{arm1} \geq 1$, $n_{arm2} \geq 1$) and for part of the running it was necessary to employ a more restrictive trigger by requiring at least two particles in the direction of the outgoing antiproton bunch ($n_{arm1} \geq 2$, $n_{arm} > 1$) to increase the ratio of pp events to background events. By requiring at least one hit in both arms of the trigger system, single diffraction dissociation reactions have been excluded from our event sample. We estimate that 95 ± 3% of the remaining inelastic cross section is seen by the trigger.

Run conditions

Typically one bunch of $\sim 5 \times 10^{10}$ protons was colliding in our intersection region LSS4 with one bunch of initially $\sim 10^{9}$ antiprotons, giving a starting luminosity of 2×10^{25} cm^{-2} s^{-1}. The luminosity lifetime was usually limited by the lifetime of the antiproton bunch which varied from one to ten hours. The beam conditions in connection with our trigger system yielded on average $\sim$ 25% of beam-beam interactions amongst the pictures taken. A summary of the trigger conditions and the data taken is given in table 1.

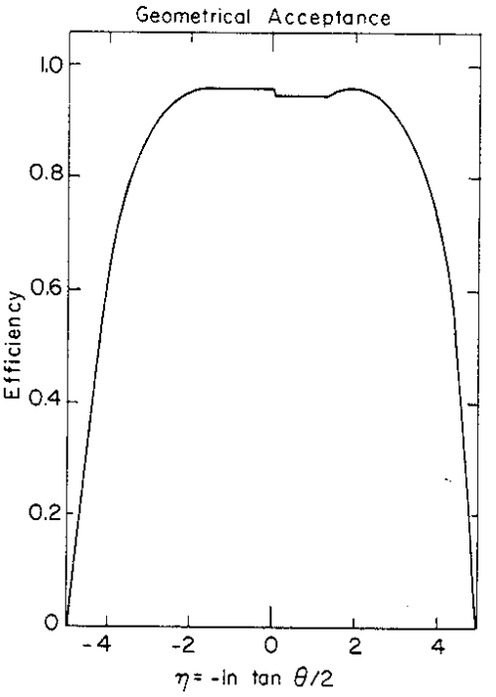

Fig. 2 - Geometrical acceptance of the streamer chamber system as a function of pseudorapidity

DATA ANALYSIS

An example of a complete event as seen by the two supplementary cameras is shown in figs 3 and 4. The events recorded on film are analysed in the following way: the film is first scanned in order to eliminate obvious background events. Each track of the event candidates found is then digitized, and reconstructed in space with the analysis program already tested in an ISR experiment [3]. The sample of measured events used for this report amounts to $\sim$ 350, involving a total of 17 000 tracks. A computer display of a measured and reconstructed event is shown in fig. 5.

Table 1 - Summary of data taken at the Collider in period 7 and running conditions

Run	No. pix	Trigger	% good pp events	No. $p\bar{p}$ inter'ns	$\mathcal{L}_{init}$
21-22 October	20 100	$arm1_{n\geq 1} \cdot arm2_{n\geq 1}$	0-40 (av. $\sim$ 16)	3200	$\sim 1\ 10^{25}$
6-10 November	39 800	$arm1_{n\geq 2} \cdot arm2_{n\geq 1}$	20-85 (av. $\sim$ 33)	13000	$\sim 2\ 10^{25}$
TOTAL	$\sim$ 60 K		$\sim$ 27%	$\sim$ 16 K	

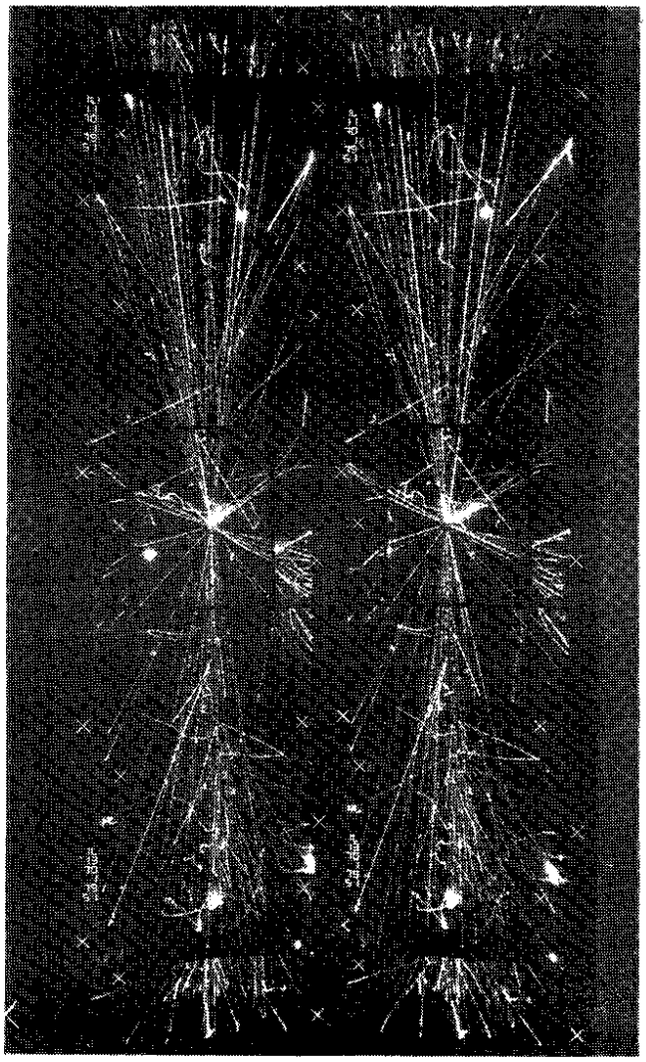

Fig. 3 - The two stereo views of an event recorded by the lower streamer chamber

Fig. 4 - The two stereo views of the same event recorded by the upper chamber

A computer program is used to separate the primary vertex from possible secondary vertices occurring in the beam pipe, and to classify primary and secondary tracks accordingly. This program has been optimized in the previous ISR experiment and by Monte-Carlo simulations of collider events using a variety of event generators. From these studies we are convinced that $\sim$ 90% of primary tracks are immediately correctly identified; the remaining 10% are confused with secondary tracks, but a cut which separates the latter ones statistically was able to reduce the uncertainty on the number of primaries to $< 5\%$. The Monte-Carlo program corrects for the remaining uncertainty and for the acceptance of the apparatus, for secondary nuclear interactions, decays of particles, multiple scattering, pair conversions, bremsstrahlung, δ-rays down to $\sim$ 1 MeV and for the measurement errors.

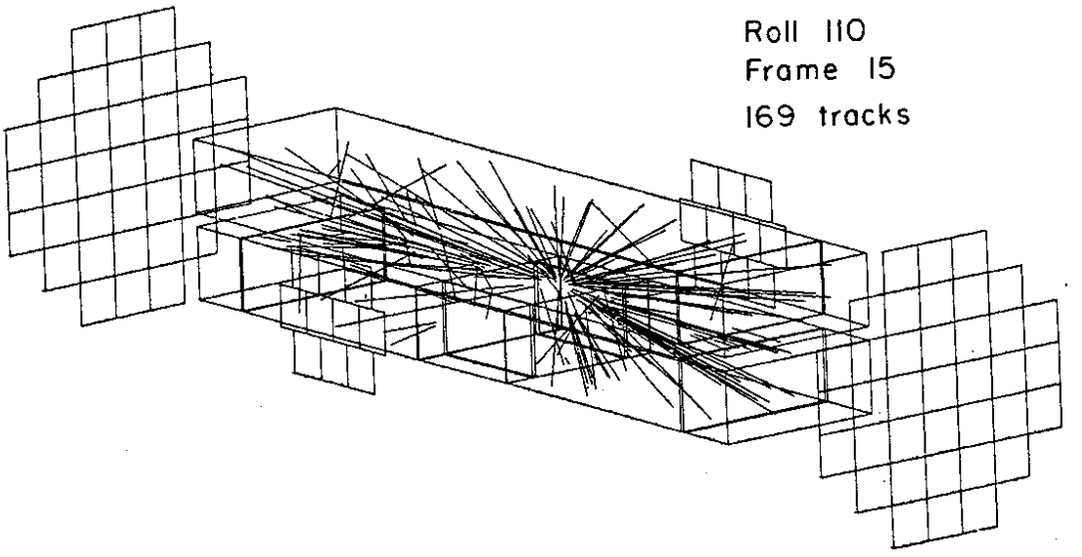

Fig. 5 - Computer display of a meausured and reconstructed event with very large multiplicity.

The distribution of identified primary vertices perpendicular to the beam direction is shown in fig. 6. The width of this distribution is 3 mm and 4 mm in the y and z directions respectively. Event candidates with primary vertices such that $|z| \geq 2$ cm, where z is the depth coordinate measured from the median plane of the beam pipe, are likely to result from interactions of beam halo particles in the beam pipe material and have been excluded. A distribution of primary vertices along the beam direction for one collider run is shown in fig. 7. The two bumps separated by 75 cm are due to the fact that the antiprotons were spread over two RF buckets in that particular run.

In view of the observed complexity of the events and the

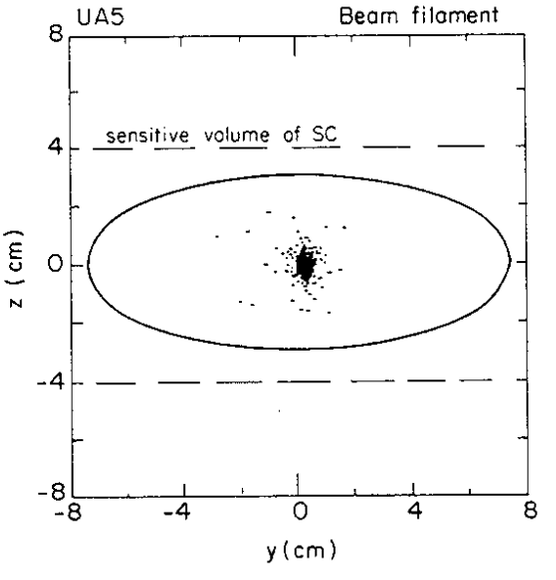

Fig. 6 - Reconstructed primary vertex positions in the plane vertical to the beam direction. The elliptical beam pipe and the sensitive volume of the two chambers are indicated.

possibility of unusual phenomena we have analyzed ∿ 100 events by a completely independent method. In this method the events were carefully scanned by physicists and the tracks pointing to the primary vertex were identified and their pseudo-rapidities determined using a template. Clear cases of e^+e^- pairs from γ conversions were eliminated. The identification of primary tracks was fairly unambiguous with an accuracy of ∿ 0.1 units in rapidity. To extract the true distribution of primary charged particles the data were corrected for the geometrical losses (∿ 25%), the effects of secondary interactions (∿ 1.5%), γ conversions (∿ 13%) and strange particle decays (∿ 5%).

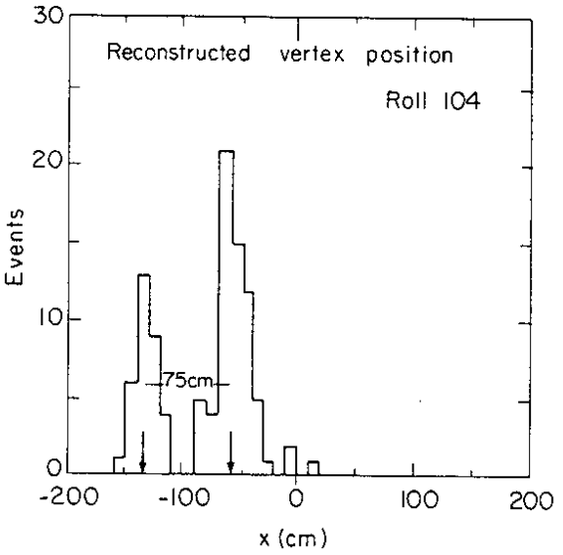

Fig. 7 - Reconstructed primary vertex positions along the beam direction. The two clusters of events result from antiprotons being spread over two RF buckets.

For calculating the necessary corrections it was assumed in both methods that all γ's come from decays of π^0's, and that $\pi^0/\pi^{ch} = 0.5$. The contamination due to strange particles decaying before entering the chambers was estimated assuming a ratio of all K's to all π's (charged and neutral) to be 0.2. No attempt has been made in the two methods to correct the loss of single diffractive events which are largely excluded by the two-arm trigger described above. Except when indicated otherwise the following results therefore refer to inelastic events, with the single diffraction dissociation component excluded. From the Monte-Carlo calculation we estimate that only 5 ± 3% of non-diffractive events have been lost by our trigger, these being of very low multiplicity.

PHYSICS RESULTS

The corrected pseudorapidity distribution folded about $\eta = 0$ is shown in fig. 8(a). We see that the distribution is generally flat over the region $|\eta| < 3$, where the average number of particles per unit rapidity is 3.0 ± 0.1. For comparison, we obtained[3] an average value 1.75 ± 0.07 for $|\eta| < 2$ at $\sqrt{s} = 53$ GeV using the same detector at the ISR. In a cosmic ray balloon experiment at approximately $\sqrt{s} \approx 180$ GeV[4], in which the charged secondaries were detected with good efficiency, the value obtained is 2.6 ± 0.5. These average values are shown in fig. 9, together with values of $1/\sigma(d\sigma/d\eta)$ ($\eta = 0$) obtained at different ISR energies[5], and lower energy FNAL values[6]. In all these experiments no trigger condition requiring at least one charged particle in the acceptance region of the central rapidity range was made, as is often the case with counter experiments. A &ns exptrapolation of all lower energy data would

suggest a central region value of $1/\sigma(d\sigma/d\eta)$ of $\sim$ 2.6 instead of the 3.0 ± 0.1 observed with our experimental set-up. This difference could well be accommodated by the possible 18 ± 5% single diffraction dissociation contribution suggested at our energy[7] to which our trigger was insensitive, leading to an equivalent renormalization of the distribution.

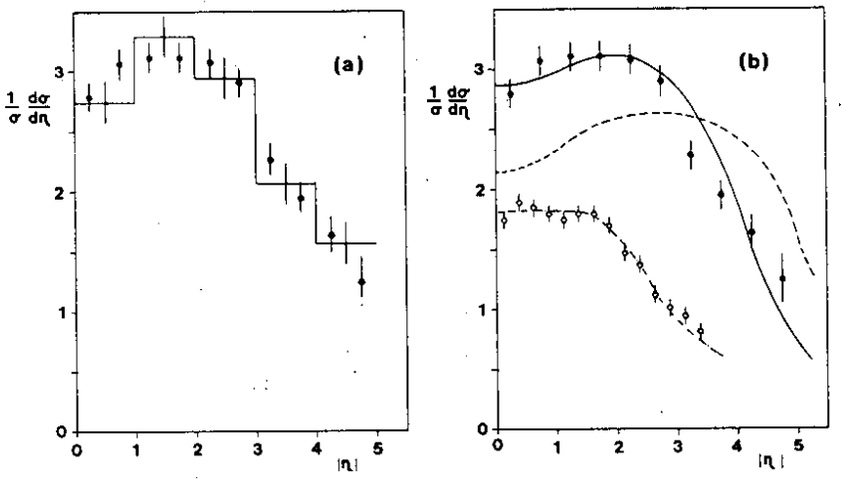

Fig. 8 (a) Corrected pseudorapidity distributions for $\sqrt{s}$ = 540 GeV folded about η = 0, from 100 events template – measured by physicists (histogram) and from 340 events passed through our digitizing and analysis procedures (solid points). The errors are statistical only. (b) Data from 340 events at $\sqrt{s}$ = 540 GeV compared with earlier UA5 data obtained at the ISR at $\sqrt{s}$ = 53 GeV (open points). The dashed and dot-dashed curves are predicted from p_t limited phase-space for $\langle p_t \rangle$ = 350 MeV/c. The solid curve for $\sqrt{s}$ = 540 GeV is from the same model but for $\langle p_t \rangle$ = 500 MeV/c.

The central plateau in rapidity in fig. 8 appears to extend to ± 3 units, so that by $|\eta|$ = 4.25 the distribution has fallen to half its maximum value. For comparison at $\sqrt{s}$ = 53 GeV[3] the plateau was ± 2 units wide, and fell to half maximum at $|\eta| \simeq 3.25$. So we observe that the width of the plateau has grown by only $\sim$ 2 units in going from $\sqrt{s}$ = 53 GeV to $\sqrt{s}$ = 540 GeV, whereas the separation of the two beam particles has increased by 4.6 units over this energy. Thus, the central plateau has not spread as much as it could have done on kinematic grounds.

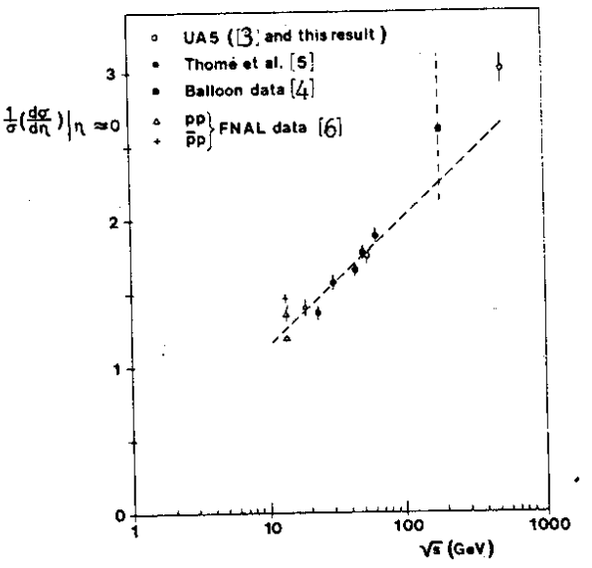

Fig. 9 Charged particle density in pseudorapidity near η = 0 from various experiments up to Collider energy. Our Collider value is for single diffractive events excluded. The straight line is drawn by eye to indicate a possible ln s dependence of the lower energy data. The values from the ISR of ref. [5] were obtained by reading off at η = 0 from fig. 6 of that reference.

Using the conventional cylindrical phase space description with $\langle p_t \rangle$ = 350 MeV/c, assuming that leading baryons take on the average half the energy of the

incoming particles and taking the particle ratios measured at the ISR[8] we can nicely reproduce our ISR data as shown in fig. 8(b). Taking this model and assuming that the particle ratios extrapolate smoothly to collider energies leads to the dashed curve of fig. 8(b). We see immediately that the central rapidity plateau is expected to extend to ≈ 5 units in such a model. Furthermore, the curve predicts a significant dip near $|\eta| = 0$. It is evident from the comparison that such a description cannot account for the data. We would have to increase p_t to ≈ 500 MeV/c, as shown in the solid curve, to get reasonable agreement. In the cosmic ray data[4] referred to earlier, a reliable measurement of energy is done only for the γ-rays in the forward hemisphere; from these measurements $\langle p_t \rangle$ for π^0's was found to be 400 ± 20 MeV/c.

Using the ∿ 350 measured events we have determined the multiplicity distribution of charged particles. The distribution of the raw data i.e. the primary tracks which were associated with the interaction vertex is shown in fig. 10(a). The distribution of the charged particles shows a pronounced tail which extends to more than three times the average. Mean value and dispersion are given in table 2.

Table 2

Values of $\langle n_{ch} \rangle$, $D = \langle (n - \langle n \rangle)^2 \rangle^{1/2}$ and $\langle n_{ch} \rangle / D$ obtained from the measured charged particle multiplicity at $\sqrt{s}$ = 540 GeV. The left-hand column refers to the measured distributions before corrections were applied. The corrected values appear in the next two columns: firstly we give the values under our trigger conditions, i.e. single diffraction excluded, and then in the last column we give values of $\langle n_{ch} \rangle$ allowing for a diffractive component (see text).

Quantity	Raw data	Corrected data	
		Single diffraction dissociation excluded	Single diffraction dissociation allowed for
$\langle n_{ch} \rangle$	20.0 ± 0.7	28.0 ± 2.0[(a)] 26.8 ± 2.1[(b)]	21 to 27
D	11.2 ± 0.5	12.5 ± 1.7[(a)]	-
$\langle n_{ch} \rangle / D$	1.8 ± 0.2	2.2 ± 0.3[(a)]	-

(a) After unfolding the smearing of multiplicity due to acceptance limitations.

(b) From a simple integration of the pseudorapidity distribution.

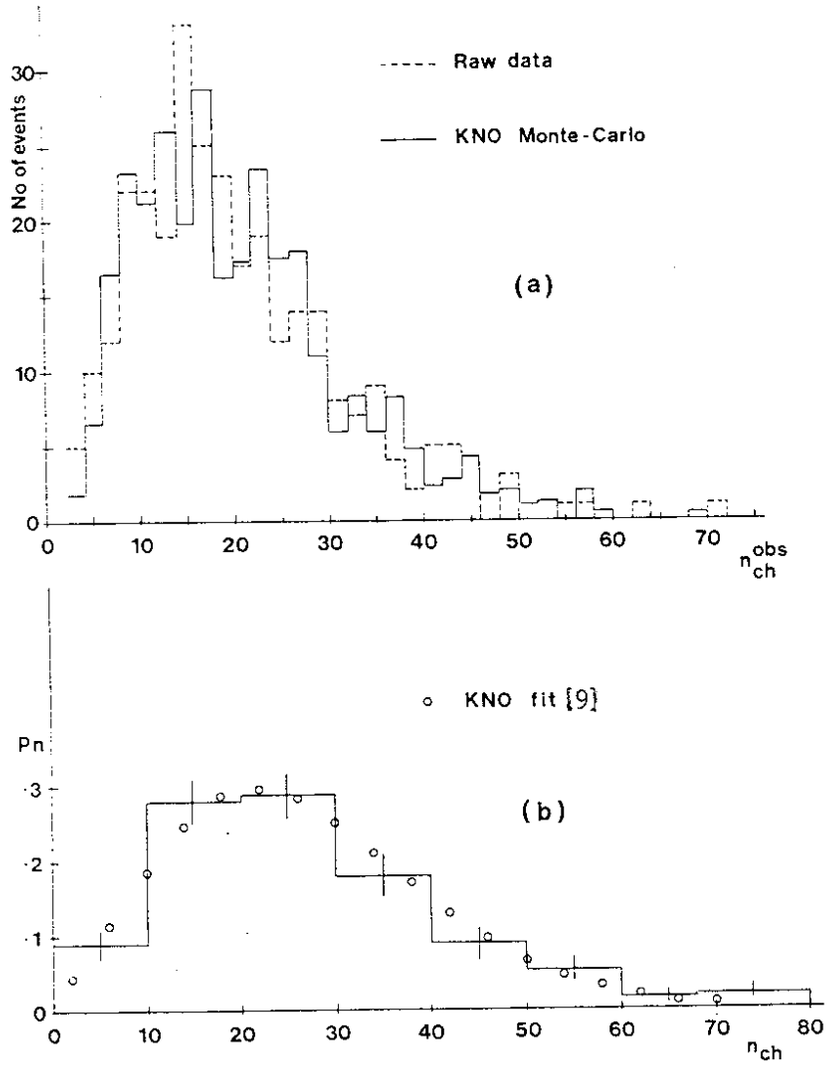

Fig. 10 - (a) Charged particle multiplicity for raw data obtained in this experiment by associating observed primary tracks to the interaction vertex, compared with a Monte-Carlo prediction following KNO scaling obtained after tracking through our detector. (b) Measured multiplicity distribution corrected for acceptances, with KNO prediction superimposed.

For comparison we have generated events according to the model described above with a KNO distribution, following the parametrization of Slattery[9], being used for charged particles. All particles of these events have been tracked through the detector configuration and were analyzed by the same program chain as the real data. Fig. 10(a) shows as the full histogram the distribution resulting from this procedure. It is seen to be compatible with the data.

Fig. 10(b) shows the multiplicity distribution corrected for acceptances. The values of the mean charged multiplicity and the dispersion for this distribution are also given in table 2 for comparison. The KNO curve using the parameters given by Slattery[9] is superimposed on the distribution.

An independent estimate of the average observed charged multiplicity $\langle n_{ch} \rangle$ is obtained by integrating our pseudorapidity distribution given above. The value obtained is 25.2 ± 1.4. The Monte-Carlo simulation suggests that 6 ± 3% of the charged particles produced non-diffractively have $|\eta| > 5$. Taking this into account, the corrected mean charged multiplicity is therefore

$$\langle n_{ch} \rangle^{nd} = \sum n \sigma_n^{nd} / \sigma^{nd} = 26.8 \pm 2.1,$$

where the superscript nd indicates that our trigger excludes single diffraction dissociation. The above value is also given in table 2. Our best estimate is $\langle n_{ch} \rangle^{nd}$ = 27.4 ± 2.0 obtained by averaging the two values in table 1. The fit to the ISR data of Thomé et al.[5] using an $s^{1/4}$ dependence gives $\langle n_{ch} \rangle \approx 40$, a number which even at this stage we can rule out.

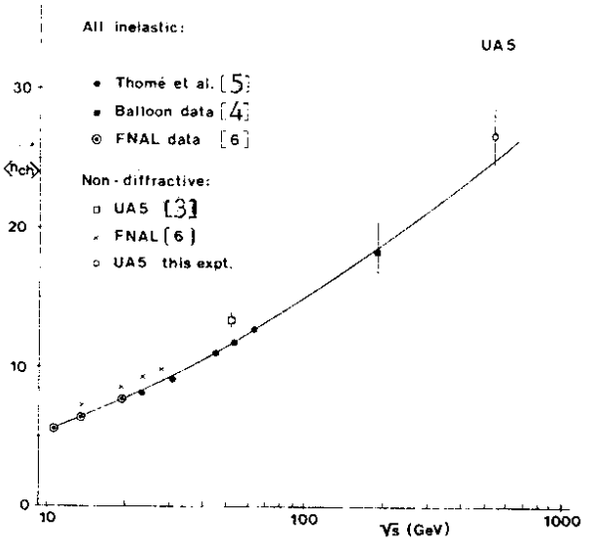

Fig. 11 Dependence of $\langle n_{ch} \rangle$ upon $\sqrt{s}$ as measured in lower energy experiments together with the Thomé et al. [1] fit of the form $\langle n_{ch} \rangle = a + b \ln s + c \ln^2 s$ to ISR and lower energy data. The UA5 data point reported here is for single diffraction dissociation excluded, and several lower energy non-diffractive vlues are also shown for comparison.

Fig. 11 shows the dependence of n_{ch} on s for several FNAL[6] and ISR[5] experiments. The data points are well described by the parametrization $\langle n_{ch} \rangle$ = $a + b\ell n s + c\ell^2 n s$ determined by Thomé et al.[5]. The value of $\langle n_{ch} \rangle$ for a recent balloon flight experiment[4] also lies well on the extrapolated curve. However, since our measured value excludes the single diffractive cross section it cannot be compared directly with the other experiments which give a value of $\langle n_{ch} \rangle$ for the whole inelastic cross section.

For FNAL data[6] and for our earlier ISR experiment[3] the values of $\langle n_{ch} \rangle^{nd}$ are also shown in fig. 11. Judging the observed difference between $\langle n_{ch} \rangle^{nd}$ and $\langle n_{ch} \rangle$ over their energy range, the difference between our measured value and the extrapolation of Thomé et al. can easily be accounted for by a single diffraction dissociation component.

To estimate the influence of diffraction dissociation[7] we assume that, as observed at the ISR, elastic scattering and single diffraction dissociation each contributes 18% to the total cross section. Making the extreme assumptions for the mean charged multiplicity $3 \lesssim \langle n_{ch} \rangle^{sd} \lesssim 1/2\langle n_{ch} \rangle^{nd}$, where the superscript sd denotes single diffraction dissociation, this leads to an estimate for the average inelastic charged multiplicity in the range $21 \lesssim \langle n_{ch} \rangle \lesssim 27$, in reasonable agreement with the prediction $\langle n_{ch} \rangle \approx 25$ of Thomé et al. This result puts in doubt speculations arising from cosmic ray studies about very high average multiplicities at collider energies. We do observe events of very high multiplicity as may be seen from figs 3 and 4, but the high multiplicity tail of the distribution needs further study.

Though we do not observe scaling in pseudorapidity (in the following simply called rapidity) by going from ISR to collider energies and there are indications that the average value of transverse momentum is rising, it seems that the multiplicity distribution when shown as a function of $z = n/\langle n \rangle$ stays essentially unchanged between $\sqrt{s}$ = 10 GeV and 540 GeV. At all energies the distribution shows a pronounced tail towards large multiplicities. This tail reflects the existence of strong correlations among the final state particles, and analyzing them could yield further insight into the dynamics responsible for particle multiplicities in the final state.

The existence of significant correlations between particles which have small separations in rapidity (up to two units) is well established at FNAL and ISR[10] energies. These correlations are energy independent and can be understood in terms of resonance production. Also energy dependent "long-range" correlations in the rapidity plateau have been observed over the ISR energy range[11] with a less clear dynamical origin.

An elegant and intuitive analysis of correlations among particles can be done in the following way[11]: let us define as "right hemisphere" the one with positive c.m.s. rapidity and as "left hemisphere" the opposite one. So-called left-right correlations can then be defined as the dependence of the average charged multiplicity $\langle n_L \rangle$ in certain rapidity intervals of the left hemisphere on the multiplicity n_R in the corresponding intervals of the right hemisphere:

$$\langle n_L \rangle = f(n_R)$$

The derivative

$$f' = d\langle n_L \rangle / dn_R$$

then measures how strongly the multiplicities in the selected rapidity intervals are correlated and this obviously can be interpreted as a measure of correlations among the particles itself.

In order to separate contributions to the left-right correlations from short-range and long-range type we define the following two sub-regions within the hemispheres:

(a) $|\eta| < 1$

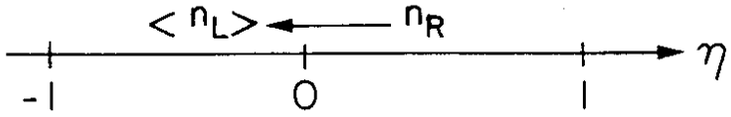

Contributions from short-range correlations like cluster or resonance decays are dominant.

(b) $1 < |\eta| < 4$

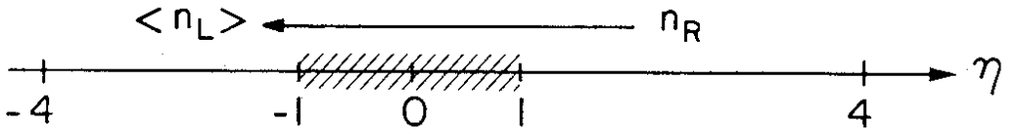

Introducing the gap of two units in rapidity eliminates contributions from short-range correlations and one is therefore only sensitive to long-range correlations.

The left-right correlations for the two intervals $|\eta| < 1$ and $1 < |\eta| < 4$ are shown in figs 12 and 13. In both cases the dependence of $\langle n_L \rangle$ on n_R seems to be compatible with a linear form $\langle n_L \rangle = a + bn_R$ where the slope b measures the strength of short and long-range correlations respectively as explained above. The energy dependence of the observed correlations is investigated by a comparison with the equivalent data from the ISR[11] (fig. 14). The strength of short-range correlations indicated by circles in fig. 14 shows no significant rise over the entire range of 20 GeV $\lesssim \sqrt{s} \lesssim$ 540 GeV. A possible explanation of this would be that the percentage of particles coming from resonance or cluster decays and their decay multiplicity is about the same over this energy range. On the other hand the strength of long-range correlations which are negligible at ISR energies when compared with short-range correlations, have grown substantially at collider energies (see squares in fig. 14). This increase seems to be roughly compatible with an extrapolation of the observed energy dependence over the ISR energy range.

Summarizing this correlation analysis one can say the following: short- and long-range correlations seem to be of equal importance at collider energies. This can be looked at in the following way. If one requires a large (small) multiplicity in a certain region of rapidity the tendency (as measured by the slope b) to observe a large (small) multiplicity in an adjacent bin of rapidity and a bin further away is about equally high. Certainly energy-momentum conservation also contributes to the observed long-range correlation. A study of the importance of this influence is under way.

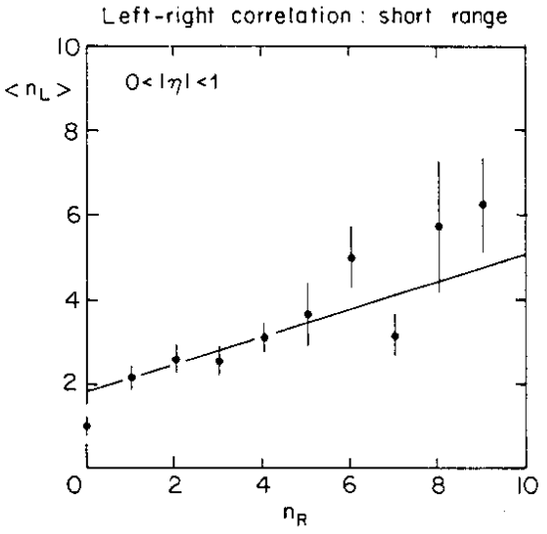

Fig. 12 - Average charged multiplicity in the rapidity interval $-1 < \eta < 0$ as a function of charged multiplicity in the corresponding interval of positive rapidity. A straight line fit to the data is indicated.

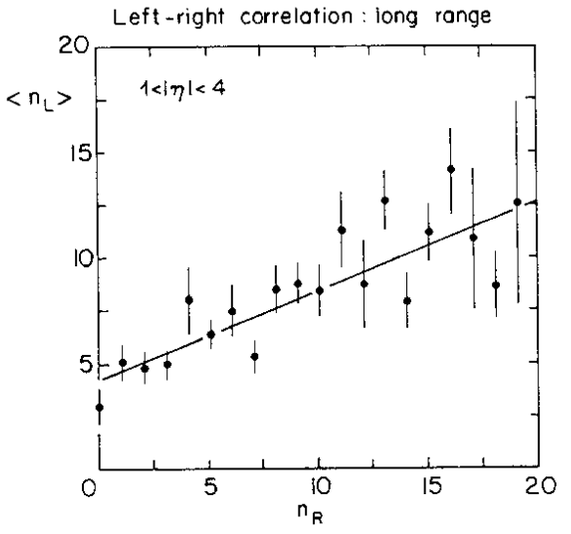

Fig. 13 - Average charged multiplicity in the rapidity interval $-4 \lesssim \eta \lesssim -1$ as a function of charged multiplicity in the corresponding interval of positive rapidity. A straight line fit to the data is indicated.

We have also studied the production of photons in the region of the central lead-glass plates (see paragraph: apparatus) which cover the two central units of rapidity, $|\eta| \lesssim 1$ and about a quarter of the azimuth, $\Delta\phi \simeq 90°$. In order to analyze the correlations between the number of charged particles and photons we have also counted the charged particles in the same region. About 700 events have been analyzed with at least one photon or charged particle hitting the plates.

For charged particles the acceptance correction has been done as described before. The main corrections for photons come from the conversion probability in the lead-glass plates ($1X_0$). For the calculation of conversion probability it is necessary to fix the energies of the photons. This has been done by assuming that all photons result from π^0's with an average transverse momentum of 500 MeV/c.

In fig. 15 the average number of photons is shown as a function of n_{ch}. A linear dependence of the form $\langle n_\gamma \rangle = (1.2 \pm 0.2) + (0.5 \pm 0.1) n_{ch}$ is compatible with the data. From the same analysis we have determined $\langle n_\gamma \rangle / \langle n_{ch} \rangle = 1.2 \pm 0.1$. The highest charged multiplicities observed on the plates of about 10 correspond to events with $\sim$ 70 charged particles being produced which is more than two times the average (27.4). But at the present status of the analysis no conclusion about the existence of Centauro events is possible.

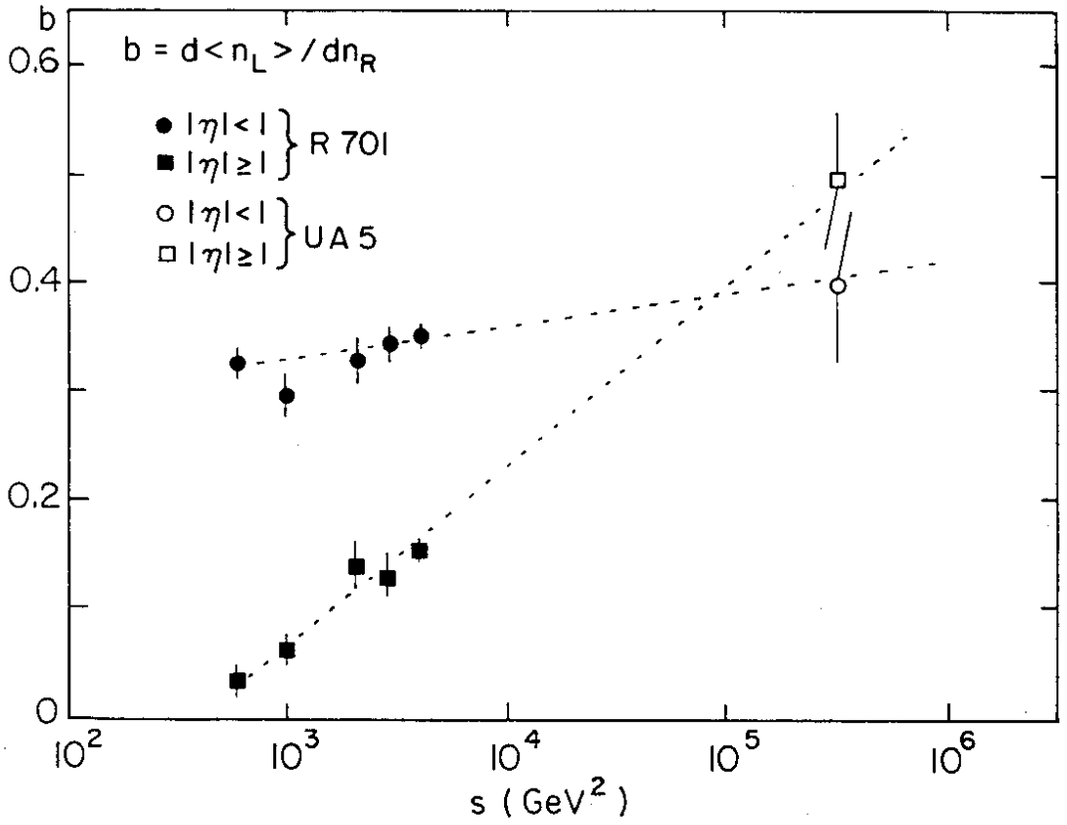

Fig. 14 - Dependence of short- and long-range correlations upon s as measured by the derivative $d\langle n_L\rangle/dn_R$ (see text). The collider data points are indicated by open symbols. The lower energy ISR data are from ref. 1. The dashed lines are shown to guide the eye.

CONCLUSIONS

We have measured non-diffractive charged particle production in $p\bar{p}$ interactions at $\sqrt{s}$ = 540 GeV over the rapidity range $|\eta| < 5$. An average value for the central rapidity density of 3.0 ± 0.1 has been found. A comparison with ISR data shows that the width of the η distribution has not increased as much as the separation of the two beam particles. A conventional cylindrical phase space model could accommodate this by increasing the p_t from 350 MeV/c to 500 MeV/c. The observed average charged multiplicity of 27.4 seems to be compatible with the parametrization of Thomé et al. for lower energies if we allow for single diffraction dissociation. An $s^{1/4}$ dependence of $\langle n_{ch}\rangle$ seems to be ruled out. The distribution of charged multiplicities, showing a pronounced tail towards large multiplicities is compatible with KNO scaling within the present accuracy of the data. Short-range correlations between charged particles with similar strength as observed at the ISR have been found. Long-range correlations which extend over more than two units in rapidity are of comparable strength to the short-range correlations. In the central region the ratio $\langle n_\gamma\rangle/\langle n_{ch}\rangle$ is close to 1 and a linear dependence of $\langle n_\gamma\rangle$ on n_{ch} over a wide range of charged multiplicity seems to hold.

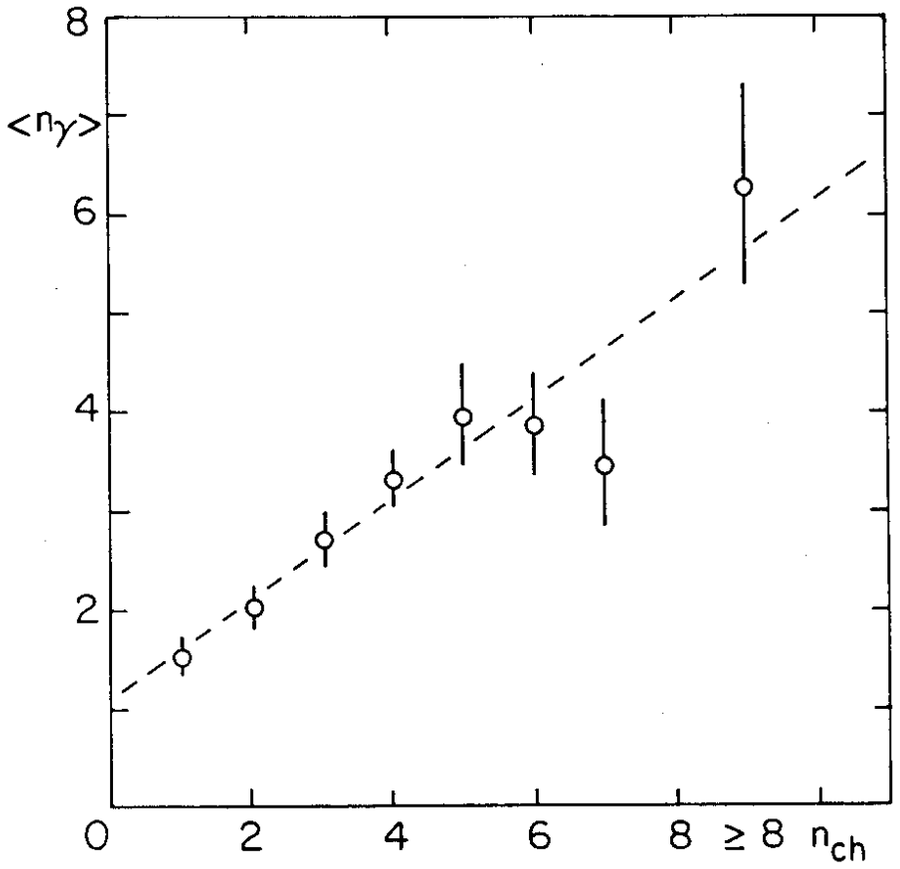

Fig. 15 - Average number of photons in $|\eta| \lesssim 1$ and $\Delta\phi \approx 90°$ as a function of multiplicity in the same interval. The dashed line shows a linear fit to the data

REFERENCES

1. K. Alpgard et al., Phys. Lett. 107B (1981) 310, 315.

2. UA5 Collaboration, Bonn-Brussels-Cambridge-CERN-Stockholm, Physica Scripta 23 (1981) 642.

3. K. Alpgard et al., Comparison of $p\bar{p}$ and pp Interactions at $\sqrt{s}$ = 53 GeV, to be submitted to Phys. Lett.

4. S. Tasaka et al., University of Tokyo, Institute of Cosmic Ray Research, preprint ICR 93-81-9.

5. W. Thomé et al., Nucl. Phys. B129 (1977) 365.

REFERENCES (Cont'd)

6. C.P. Ward et al., 100 GeV/c $p\bar{p}$, Nucl. Phys. B153 (1979) 299;
C. Bromberg et al., 100 GeV/c pp, Phys. Rev. D9 (1974) 1864;
W.M. Morse et al., Phys. Rev. D15 (1977) 66;
J. Whitmore et al., 205 GeV/c pp, Phys. Rev. 10C (1974) 273;
A. Firestone et al., 303 GeV/c, Phys. Rev. D10 (1974) 2080;
C. Bromberg et al., 405 GeV/c pp, Phys. Rev. Lett. 31 (1973) 1563.

7. G. Goggi et al., Proc. XII Rencontre de Moriond (Flaine, 1977), ed. J. Tran Than Van;
G. Alberi and G. Goggi, Phys. Rep. 74 (1981) 1.

8. G. Giacomelli and M. Jacob, Phys. Rep. 55 (1979) 41.

9. P. Slattery, Phys. Rev. D1 (1973) 2073.

10. S.R. Amendolia et al., Phys. Lett. 48B (1974) 359;
S.R. Amendolia et al., Nuovo Cim. 31A (1976) 17;
C. Bromberg et al., Phys. Rev. D10 (1974) 3100;
K. Eggert et al., Nucl. Phys. B86 (1975) 201;
B.Y. Oh et al., Phys. Lett. 56B (1975) 400;
R. Singer et al., Phys. Lett. 49B (1974) 481.

11. S. Uhlig et al., Nucl. Phys. B132 (1978) 15.